PROCEEDINGS OF SPIE

SPIEDigitalLibrary.org/conference-proceedings-of-spie

BEaTriX--the Beam Expander Testing X-Ray facility for testing ATHENA's SPO modules: progress in the realization

B. Salmaso, S. Basso, E. Giro, D. Spiga, G. Sironi, et al.

B. Salmaso, S. Basso, E. Giro, D. Spiga, G. Sironi, G. Vecchi, M. Ghigo, G. Pareschi, G. Tagliaferri, M. Uslenghi, M. Fiorini, L. Paoletti, C. Ferrari, S. Beretta, A. Zappettini, M. Sanchez del Rio, C. Pelliciari, V. Burwitz, I. Ferreira, M. Bavdaz, "BEaTriX--the Beam Expander Testing X-Ray facility for testing ATHENA's SPO modules: progress in the realization," Proc. SPIE 11119, Optics for EUV, X-Ray, and Gamma-Ray Astronomy IX, 111190N (9 September 2019); doi: 10.1117/12.2530430

SPIE.

Event: SPIE Optical Engineering + Applications, 2019, San Diego, California, United States

BEaTriX, the Beam Expander Testing X-ray facility for testing ATHENA's SPO modules: progress in the realization

B. Salmaso[1a], S. Basso[a], E. Giro[a,c], D. Spiga[a], G., Sironi[a], G.Vecchi[a], M.Ghigo[a], G. Pareschi[a], G. Tagliaferri[a], M. Uslenghi[b], M. Fiorini[b], L. Paoletti[c], C. Ferrari[d], S. Beretta[d], A. Zappettini[d], M. Sanchez del Rio[e], C. Pelliciari[f], V. Burwitz[g]f I. Ferreira[g], M. Bavdaz[g]

[a]INAF Astronomical Observatory Brera, Via E. Bianchi 46, 23807 Merate, Lecco (Italy)
[b]INAF-IASF Milano, Via A. Corti 12, 40133 Milano (Italy)
[c]INAF Astronomical Observatory Padova, Vicolo Osservatorio 5, 35122 Padova (Italy)
[d]CNR-IMEM, Parco Area delle Scienze 37/A, 43124 Parma (Italy)
[e]European Synchrotron Radiation Facility, B.P. 220, 38043 Grenoble (France)
[f]Max-Planck-Institüt für extraterrestrische Physik, Garching (Germany)
[g]ESTEC, European Space Agency, Keplerlaan 1, 2201 AZ Noordwijk (Netherlands)

ABSTRACT

The ATHENA X-ray telescope comprises an optical system with several hundreds of Silicon Pore Optics (SPO) Mirror Modules (MM) to be assembled. All the MMs have to be tested for acceptance before integration. INAF-Osservatorio Astronomico Brera is building in its premises of Merate (Italy) a unique pathfinder facility, BEaTriX, which is characterized by a broad (170 × 60 mm^2), uniform and parallel X-ray beam (divergence ≤ 1.5 arcsec HEW) at the energies of 1.49 and 4.51 keV. BEaTriX prime goal is to prove that it is possible to perform the acceptance tests (PSF and Aeff) of the ATHENA SPO MM's at the production rate of 3 MM/day. The system is very compact (9 x 18 m^2) and it is designed with modular compartments where the vacuum can be broken independently to replace the optics under test. It works at a vacuum level of 10^{-3} mbar, easily evacuated in a short time. The expanded and parallel beam is obtained with an X-ray microfocus source placed in the focus of a paraboloidal mirror, a monochromation stage with 4 symmetrically cut crystals, and an expansion stage where the beam is diffracted and expanded by an asymmetrically-cut crystal. The key axes of all the optical components are motorized in vacuum for a proper beam alignment. The expanded beam fully illuminates the aperture of the MMs, imaging the focused beam at 12 m distance on a CCD camera, with the sensor in vacuum and motorized in air for XYZ movements. A thermal box is also present to radiatively heat the MM and check its optical performances under different temperatures. The design of the facility started in 2012 and has been finalised under an ESA contract. After completing the design, the facility is now in the realization phase. This paper provides an overview of the current status of the facility realization.

Keywords: ATHENA, BEaTriX, X-ray testing, X-ray microfocus source, beam expander, asymmetric diffraction

1. INTRODUCTION

ATHENA (Advanced Telescope for High-ENergy Astrophysics) is the second Large mission selected by ESA within the Cosmic Vision Program [1], with launch foreseen for 2031. The optics consists of a large aperture X-ray mirror with a diameter of 2.4 m, effective area of 1.4 m^2 at 1 keV, and half-energy width (HEW) of 5 arcsec at 1 keV [2], based on the Silicon Pore Optics (SPO) technology [3], developed at Cosine (https://www.cosine.nl/, The Netherlands). To create the aperture of such a large X-ray telescope, a modular approach is foreseen, where each step of the process has to be followed by dedicated tests and calibration procedures.
35 processed silicon plates are stacked, with dedicated robotic machines, to form an X-ray Optical Units (XOU). 4 XOUs are aligned and integrated in the SPO Mirror Module (MM) using synchrotron radiation at the XPBF 2.0 beamline at the BESSY II facility in Berlin, Germany [4]. The MMs are, at present, characterized at XPBF 2.0 and at

[1] bianca.salmaso@brera.inaf.it; phone +39-039-5971028; fax +39-039-5971001; www.brera.inaf.it

Optics for EUV, X-Ray, and Gamma-Ray Astronomy IX, edited by Stephen L. O'Dell, Giovanni Pareschi, Proc. of SPIE Vol. 11119, 111190N · © 2019 SPIE · CCC code: 0277-786X/19/$21 · doi: 10.1117/12.2530430

the PANTER long beam facility of the Max-Planck-Institut für Extra-terrestrische Physik located near Munich [5]. The MMs will be aligned and integrated in the Mirror Assembly Module (MAM) by Media Lario (https://www.medialario.com/, Italy) with UV light illumination [6]. Finally, the MAM has to be calibrated. Different solutions are under consideration, including an extended PANTER [7], the XRCF facility at MSFC (USA), or a vertical facility that is now under study by INAF in collaboration with the EIE group, Media Lario, and other Italians companies [8], together with ESA.

For what concerns the MM, an accurate and fast acceptance testing is required to satisfy the fast production rate foreseen for the SPO. XPBF 2.0 and PANTER are used at the moment, but they have different limitations when considering the test of the several hundreds of MMs composing the MAM [9,10]. To overcome these limitations, INAF-Osservatorio Astronomico Brera has started in 2012 to design a unique pathfinder facility, BEaTriX (Beam Expander Testing X-ray), which is characterized by a broad (170 mm x 60 mm), uniform and parallel X-ray beam (divergence ≤1.5 arcsec HEW) at the energies of 1.49 and 4.51 keV [9, 10, 11, 12, 13, 14]. The project was at first financed by an AHEAD (Activities for the High-Energy Astrophysics Domain) grant awarded from H2020 [15], and by other dedicated INAF funds. Since 2018, the development of BEaTriX is also funded by ESA with a dedicated contract. The goal of this activity is to prove that it is possible to perform the acceptance tests (PSF and Aeff) of the ATHENA SPO MM's with the required accuracy, meaning a uniform, stable and parallel beam, and a calibration rate of 3 MM/day. BEaTriX is currently developed for the 4.51 keV energy, in a second phase it will be extended to the 1.49 keV.

The beam properties of BEaTriX are obtained with the optical design shown in Figure 1 for the 4.51 keV line, and already presented in [9,10]. A parallel X-ray beam (4 mm x 60 mm) is emerging from a parabolic mirror in the focus of an X-ray micro-focus source with a Titanium anode. The beam is then diffracted four times on Silicon crystals symmetrically cut with orientation (220): by this means, the monochromation level is very high, producing a beam with bandwidth 0.03 eV. Such a tight monochromation is necessary to minimize the effect of the energy dispersive properties of the beam expander component [16]. Beam expansion is reached by an asymmetrically cut Silicon crystal (220) with asymmetry angle (α) and Bragg angle (φ_B) chosen to obtain an expansion factor of about 50 [14], and producing a final beam of size 170 mm x 60 mm.

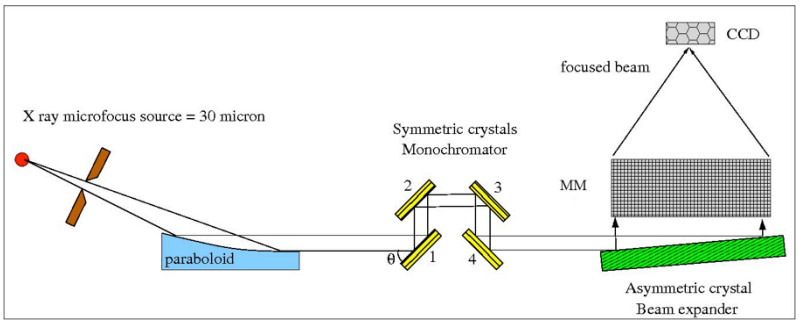

Figure 1. Optical design

A similar design will be used for the 1.49 keV line, adopting an X-ray micro-focus source with an alloy of Aluminum and Titanium for the anode [14], and the Ammonium Dihydrogen Phosphate (ADP), produced by Saint Gobain (https://www.crystals.saint-gobain.com/document/x-ray-monochromators) for the crystals. ADP crystals have been considered, among other possible choices, because of their large lattice spacing, their reported crystal quality, and because they can be grown at sufficiently large size for reasonable price. Preliminary tests have been performed [17] on ADP samples, to check the crystalline quality and lattice planarity, indicating that the ADP produced by Saint Gobain is suitable for the BEaTriX purposes.

BEaTriX will work at a fast testing rate (3 MM/day), owing a low vacuum level (10^{-3} mbar), a small vacuum system and a modular approach in the realization of the vacuum system. The mechanical design of the vacuum system has been consolidated, with respect to what initially presented in previous papers [9,10], and realized by Tecnomotive (http://www.tecnomotive.it/), an Italian company based in Padova. Figure 2 shows its design, with the components:

- two X-ray source for 4.51 and 1.49 keV (A);
- two short arms (B);
- the rectangular Optical Chamber containing the parabolic mirror (C), the symmetrically cut crystals (D), and the asymmetrically cut crystal (E);
- the Cylindrical MM Chamber where the MM under test (F) is located;
- the long arm (G);
- the CCD detector (H).

The BEaTriX coordinate reference system, shown in Figure 2, is chosen according to the ATHENA reference system.

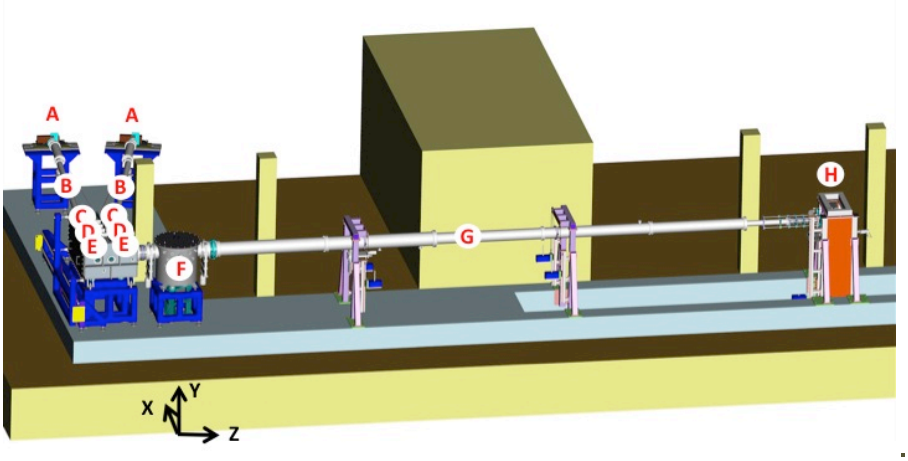

Figure 2. Mechanical design of the vacuum system, showing the optical components and the coordinate system

This paper presents the advancement status in the realization of this facility in Merate:

1) thorough simulations were performed to determine the errors sensitivity, and consolidate the contribution to the error budget. The complete analysis is presented in [18] and here summarized in Section 2, where the procurement status of the optical components is also given;
2) Section 3 presents the vacuum motorizations selected to satisfy the requirements outlined in Section 2;
3) Section 4 presents the consolidated vacuum system design, anticipated by Figure 2;
4) the vacuum pumping system for the present design is described in Section 5;
5) Section 6 briefly presents the AIV plan.
6) Section 7 deals with the control software and a simulator developed to help the progressing of the software;

Since the beginning of 2019, we entered the purchase phase, which is now on going. The BEaTriX beam line at 4.51 keV is expected to be completed by Q4 2020.

2. OPTICAL DESIGN AND ERROR BUDGET

2.1 Introduction

In the HEW error budget for the ATHENA telescope, 4.3 arcsec were allocated for each MM [19]. Testing the MM with a collimated beam, requires a collimation better than 2 arcsec. Actually, the MM's PSF is almost monodimensional, and this is relevant, for BEaTriX, because a different behavior is expected for the vertical and horizontal divergence of the X-ray beam, due to the energy dispersive behavior of the asymmetric crystal [16]. Simulations have shown [18] that the final beam divergence in BEaTriX is HEW-ver = 0.8 arcsec and HEW-hor = 1.5 arcsec, in the following conditions:

- X-ray source with focal spot of 35 µm × 35 µm and flux of 10^{11} ph/s/sr in the Ti-K_α doublet

- perfect parabolic mirror, monochromator and beam expander
- parabolic mirror with Pt coating
- first Channel Cut Crystal (CCC) rotated by 12 arcsec with respect to maximum reflectivity of the two CCC system
- perfect alignment of the optical components

A conservative 35 µm × 35 µm source size has been considered in the simulations, but the preliminary results of the Incoatec R&D work have demonstrated that a 30 µm × 30 µm size can be reached (Section 2.2). In this case HEW-ver = 0.75 arcsec and HEW-hor = 1.37 arcsec.

2.1.1 Error budget

Degradation of the beam collimation in BEaTriX can be due to:

1) not perfect quality of the optical components
2) misalignment of the optical components
3) random errors (vibrations, thermal drift)
4) detector contributions (pixel size)

The way these errors add up is not trivial to define. At the moment, our best estimate of the errors propagation is as follow:

1) the quality of the optical components
   - the finite size of the X-ray source
   - the parabolic mirror
   - the monochromator is considered as a perfect component, which is a good approximation for a silicon crystal (see Section 2.4)
   - for the beam expander, the out of planarity of the crystal planes is considered to sum linearly to the final divergence, as the curvature is a zero order deformation of the beam curvature (see Section 2.4). 0.5 arcsec is allocated for beam expander the out-of-planarity
2) alignment errors, random errors, detector errors
- these errors are considered to sum quadratically.

Table 1 shows the final beam divergence in BEaTriX, after considering the possible sources of errors: about 1.5 arcsec is expected for the vertical divergence, the most critical for testing ATHENA's MM.

Table 1: BEaTriX beam divergence error budget, for an X-ray source of size 35 µm × 35 µm

	Div-vert [arcsec]	Div-hor [arcsec]
Ideal system	0.8	1.5
Quality of the optical components	0.5	0.5
Partial beam collimation degradation (linear sum)	1.3	2.0
Alignment errors	0.5	1.0
Random errors	0.5	0.5
Detector errors	0.12	0.12
Total beam collimation degradation (quadratic sum)	1.48	2.29

In the following sections, the different contributions are discussed. In Section 2.7 a detailed error contribution is presented.

2.2 Source

The source is being produced by Incoatec (https://www.incoatec.de, Germany) for what concerns the source tube and by Gilardoni (https://www.gilardoni.it/, Italy) who will complete the source with the X-ray shield. The 4.5 keV rays are emitted by a Titanium anode; in the preliminary result, Incoatec reported measurements of the source size < 30 µm × 30

μm, with a flux > 10^{11} ph/s/sr in the Ti-K_α doublet, at a very low tube power (1.5 W). A forced air-cooling system is used (Figure 3 right).

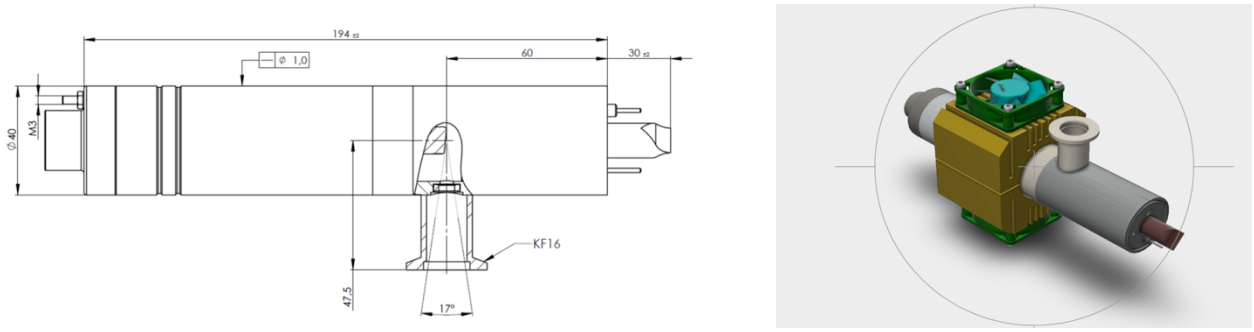

Figure 3: Left: Design sketch of the tube. Right: CAD model of the Ti microfocused tube, showing the forced air cooling system (credits Incoatec)

A conservative size of 35 μm × 35 μm and flux of 10^{11} ph/s/sr in the Ti-K_α doublet was chosen for the simulations [18], performed well before the production of the source tube.
These simulations have shown that the dependences of the vertical and horizontal divergences of the final beam, on both the source size and the source alignment, are different.
For what concerns the alignment, in the simulations we separate the six degrees of freedom in translations of the X-ray source, and rotation of the parabolic mirror. This was done with the goal to minimize the number of motors inside the vacuum system, considering alignment in air for the X-ray source and in vacuum for the parabolic mirror.

The effect of the source translations, can be summarizes as follows:

- X displacements are not critical up to ± 1 mm;
- Y displacements of 50 μm increases the vertical divergence by 0.2 arcsec, while do not change the horizontal divergence;
- Z displacements are the most critical:
    - 40/50 μm displacement increases the vertical divergence by 0.2 arcsec
    - 10/20 μm displacement increases the horizontal divergence by 0.2 arcsec

The source position adjustments in air are obtained with the plates described in Section 4.1.

2.3 Parabolic mirror

The parabolic mirror substrate was procured by Zeiss in a preliminary lapped status [9,10]. It is now being precisely figured and polished at INAF-OAB with a Zeeko bonnet polishing machine (IRP, Intelligent Robotic Polisher, 1200 model), while the metrology is performed at Media Lario. The results of the polishing obtained so far are reported in [20]. The goal is to reach a surface quality of 0.5 arcsec HEW since, in this case, there is almost no degradation to the final beam divergence. The dependence of the final beam divergence upon the quality of the parabolic mirror is fully described in [18].

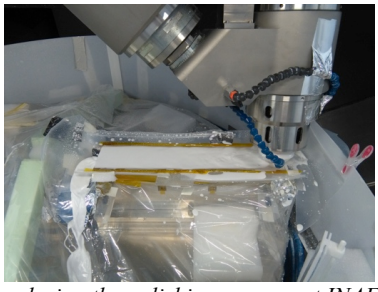

Figure 4: The parabolic mirror during the polishing process at INAF-OAB with the Zeeko machine

As for the alignment, the simulations described in [18] show the effect of rotation of the parabola with respect to the source. It is therein shown that:

- the horizontal divergence is the more affected by a rotation of the parabolic mirror
- the most critical rotation is the one in the vertical plane (rotation around the Z axis) as the one in the horizontal plane (rotation around the Y axis) can be compensated by a proper rotation of the crystals, in order to recover the correct incidence angle. A rotation of 2 arcsec in the vertical plane entails a collimation degradation of 0.25 arcsec in the horizontal direction.

2.4 Crystals: monochromator and beam expander

Symmetrically-cut crystals (i.e., with diffracting planes parallel to the outer surface) are used in BEaTriX to monochromate the beam, followed by asymmetrically-cut crystals to expand the beam in the horizontal direction. The (220) diffraction planes of Silicon crystals are used for the 4.51 keV line.
The Silicon monochromator is based on two Channel Cut Crystals (CCC), where the first can be rotated with respect to the second one (Figure 5) in order to optimize either the horizontal divergence or the flux [9,10,18]. This aspect is of particular importance for the ATHENA MMs case, where the PSF is almost monodimensional and, in the BEaTriX detector, it is spread in the vertical direction, which is the less critical [18].

The CCC in Si(220) will be soon procured, while the beam expander in Si(220) is already available (Figure 6 left) [9,10]. It has been cut at CNR-IMEM, an institute with a very long experience in X-ray diffracting crystals, from a monocrystalline cylinder in silicon (diameter = 20 cm, thickness = 50 mm) to the size of 170 mm × 60 mm × 20 mm.

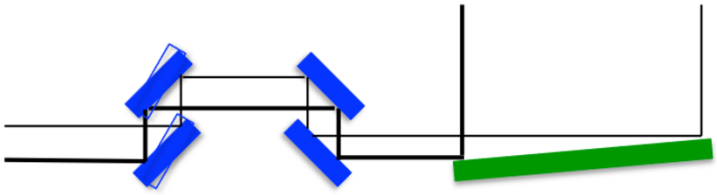

Figure 5. The optical layout of the crystals. In the monochromator (blue) the beam is diffracted 4 times on the surfaces of two CCC, where the first CCC can be rotated with respect to the second one. The beam is expanded by the asymmetrically-cut crystal (green).

Both CCC and beam expander are manufactured from monocrystalline Silicon with the following specifications:

- produced with the Float Zone method to minimize impurities
- zero etched pit density (0-EPD), corresponding to 0/cm^2 dislocation density.
- all the surfaces are lapped to remove machining damage
- all the surfaces are etched to remove residual strain from the machining

For these reasons, both crystals can be considered as perfect components to a good approximation. Due to the larger length of the beam expander (length = 170mm) with respect to the monochromator (length = 30mm), we have anyway allocated some possibility for out of planarity errors to the beam expander, i.e. 0.5 arcsec: this is expected to sum linearly to the final divergence, as the curvature is a zero order deformation of the beam curvature.

The beam expander planarity was recently measured, at CNR-IMEM, with a Philips diffractometer Xpert-pro. Both surfaces were measured and the Bragg peak displacement was used as indication of surface curvature, using the semi-difference approach (Figure 6, center and right). The Radius of Curvature (RoC) was estimated to be about 12 km, limited by the instrumental error. This value has to be compared with an estimate of RoC $\geq$ 35 km, considered to maintain the degradation of the horizontal collimation to $<$ 0.5 arcsec on a sample 170 mm long. To cop with this extremely large RoC, a more accurate system should be used, but this is not available.

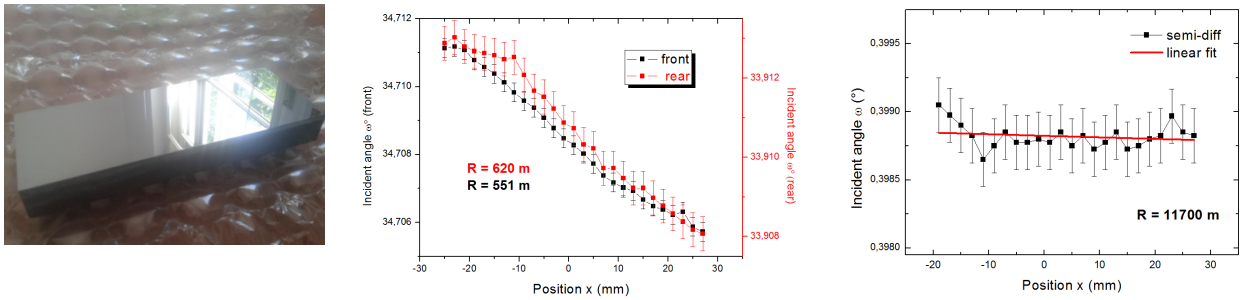

Figure 6: Beam expander. Left: the crystal cut and polished at CNR-IMEM. Center: planarity measurements: Bragg peak displacement on front and back surfaces. Right: planarity measurements: semi-difference of front and back Bragg peak

The sensitivity analysis on the alignment of the crystals is fully described in [18], and here summarized:

- monochromator:
  - pitch error: rotations of the first CCC in the horizontal plane have almost no effect for the vertical collimation, while the horizontal collimation is shown to be optimized by -12 arcsec rotation, at the expenses of flux;
  - roll error: regarding the rotation of the first CCC around a line on the crystal surface, about ± 200 arcsec can be tolerated without significant increase of the horizontal divergence;
  - yaw error: rotations of the first CCC in the vertical plane have no effect.
- beam expander:
  - the beam expander rotations do not affect the beam collimation;
  - the pitch error causes a loss of intensity of a factor 10 at +/- 100 arcsec;
  - for roll and yaw misalignment, the most notable effect is a geometrical displacement of the beam emerging from the beam expander: 20 arcsec rotation causes a beam displacement of 1.3 mm along Y, the vertical direction in the BEaTriX coordinate system (Figure 2).

2.5 Detector

The detector is a directly illuminated CCD, with a back-illuminated sensor of size 27.6 mm × 27.6 mm and pixel 13.5 µm. The finite pixel size (13.5 µm) induces a HEW degradation of half the pixel, i.e. 0.12 arcsec.

2.6 Random errors

Random errors are considered to arise from:

1) *Vibrations.* Stable foundations were designed and built with the goal to damp possible vibrations arising from anthropic sources [9,10]. It will be verified during commissioning that the system is stable within 1 pixel of the CCD (chosen of 13.5 µm = 0.23 arcsec at 12 m distance from the MM) during the integration time (estimated to be about 30 min).
2) *Thermal effects.* The major error is considered occurring when the source and parabolic mirror drift to different height. Since the room is controlled at ±1°C, considering supports of 1 m height in steel, 24 µm difference can be present at maximum in the two parts. The analysis indicates an increase of about 0.35 arcsec in the horizontal divergence.

Considering the quadratic sum of vibrations and thermal effects, and considering as more critical the thermal aspect, we allocate up to 0.45 arcsec for it, which gives a total of 0.5 arcsec to the random errors.

2.7 Contributions to the error budget

From the analysis shown in the previous Sections, we can split the contributions of the errors.
The source size is conservatively considered 35 μm × 35 μm.
The parabolic mirror quality is considered to 0.5 arcsec HEW: this does not degrades the final beam collimation.
The silicon crystals are considered perfect, as explained in Section 2.4.1. A degradation of 0.5 arcsec is anyway allocated for out of planarity of the beam expander, even if the experiments indicates that no curvature is present, as measured by the available instrument.
The misalignment contributions are derived from simulations.

Table 2: BEaTriX beam divergence error contributions, for an X-ray source of size 35 μm × 35 μm

		Div-vert [arcsec]	Div-hor [arcsec]	Note and tolerance
Ideal system		0.8	1.5	
Quality of the optical components	Parabola	0	0	Polished to 0.5 arcsec HEW
	CCC	0	0	
	Beam expander	0.5	0.5	Out of planarity
Partial beam collimation degradation (linear sum)		1.3	2.0	
Alignment errors	Source shift Y	0.25	0.25	Vert: mechanical adj. in air up to 150 μm Hor: mechanical adj. in air up to 65 μm
	Source shift Z	0.25	0.25	Vert: mechanical adj. in air up to 50 μm Hor: mechanical adj. in air up to 15 μm
	Parabola rot Y	0.25	0.25	Vert: Vacuum motor adj. up to 2 arcsec Hor: Vacuum motor adj. up to 0.5 arcsec, higher if compensated by CCC rotation
	Parabola rot Z	0.25	0.25	Vert: Vacuum motor adj. up to 10 arcsec Hor: Vacuum motor adj. up to 4 arcsec
	CCC rot X	0	0	Vert: Not critical Hor: Not critical up to ± 200 arcsec
	CCC rot Y	0	0.85	Vert: Not critical up to ± 16 arcsec Hor: Vacuum motor adj. up to 2 arcsec
	Beam Exp	0	0	Not critical for HEW but care for geometrical displacement
Random errors	Vibrations	0.23	0.23	
	Thermal	0.45	0.45	
Detector errors	Pixel size	0.12	0.12	Pixel size 13.5 μm
Total beam collimation degradation (quadratic sum)		1.49	2.29	

3. VACUUM MOTORS REQUIREMENTS AND PROCUREMENT STATUS

From the sensitivity analysis shown in [18] and in Section 2, we have derived the requirements for the vacuum motors. The type of vacuum motor systems, procured by Physik Instrumente (https://www.pionline.it/it/, Italy), are shown in Table 3. A total of 13 vacuum motorizations are considered, 11 for the optical components responsible of the beam moderation and located in the Optical Chamber, 2 for the MM, located in the MM Chamber.

Table 3: Vacuum motorizations for the optical components present in the Optical Chamber

Parabolic mirror	Monochromator and beam expander	Mirror module
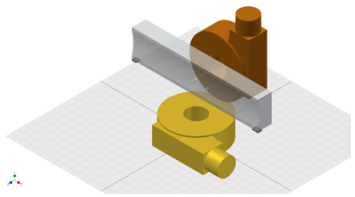	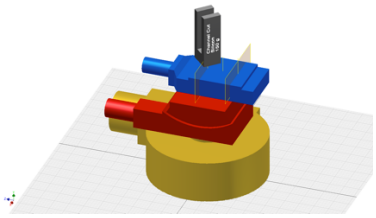	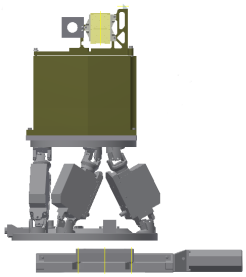
ROT Y : Resolution = 0.5 arcsec ROT Z : Resolution = 0.5 arcsec	ROT Y : Resolution = 0.5 arcsec ROT X : Resolution = 10 arcsec TRASL Z : Resolution = 0.5 µm	Hexapod Resolution XYZ = 0.3 µm Range XZ = ± 22 mm, Y = ± 12.5 mm Resolution θXθYθZ = 0.7 arcsec Range θXθZ = ± 7.5 deg, θY = ± 12.5 deg TRASL X: Resolution = 0.3 µm Range = 100 mm

4. MECHANICAL DESIGN OF THE VACUUM SYSTEM

The consolidated vacuum system layout is presented in Figure 2. A modular approach was considered, in order to have independent sectors to be evacuated. In particular, the independent evacuation of the short arms is important for the alignment procedure of the X-ray source to the parabolic mirror, which will be performed first in air with visible light, than in vacuum with X-rays; the independent evacuation of the MM Chamber is essential for a fast MM interchange. The following Sections describe the various components of the vacuum system.

4.1 Source tower

The source is mounted on an interface piece (Figure 7), able to manually rotate around the hinges of the short arm near the Optical Chamber, in order to follow the rotation of the tubes. The rotation is essential to adjust the incidence angle on the parabola and the crystals. Finer manual movements are possible to permit the source alignment. A shutter, triggered by the CCD camera, is placed in front of the source. A shutter is required as the selected camera is not frame transfer. A pinhole, positioned as close as possible to the X-ray tube, limits the angular aperture of the X-rays to the entrance pupil of the parabolic mirror.

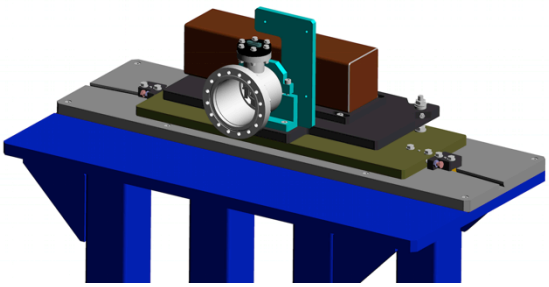

Figure 7: The source tower showing the X-ray source box (brown), the plates for the coarse arm rotation and the fine source adjustment, the house for the shutter (gray).

4.2 Short arms

The short arms connect the X-ray sources to the Optical Chamber (Figure 8). They hold near the optical chamber a gate valve to have the possibility to isolate them as independent sectors. A bellow is present to adjust the correct angle of the beam to the parabola and the crystals, by a rotation of the arms in the horizontal plane. Two flanges are present on the short arm and on the Optical Chamber, to allow the imaging of the source from the Optical Chamber, for alignment purposes (magenta lines in Figure 8).

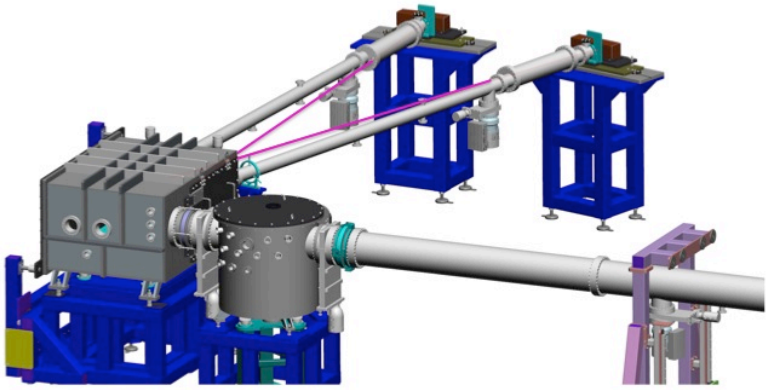

Figure 8: The short arms. The magenta lines, from the Optical Chamber to the sources indicates the alignment beam path

4.3 Optical Chamber and Mirror Module Chamber

The optical components, in charge of the beam moderation (the parabolic mirror, the monochromator and the beam expander) are positioned inside the rectangular chamber, named Optical Chamber (Figure 9). In order to install all the components and to facilitate the alignment, two sides of the chamber provide the accesses for handling the components. The rear panel is as large as the chamber and can slide laterally on a guiding system (Figure 9 right). The MM is placed inside the cylindrical tank of Figure 9 left, named MM Chamber. The optical components in both chambers are placed over an optical bench, mechanically decoupled from the vacuum chamber.
Entrance and exit of both chambers can be closed by gate valves, in order to make them independent sectors.

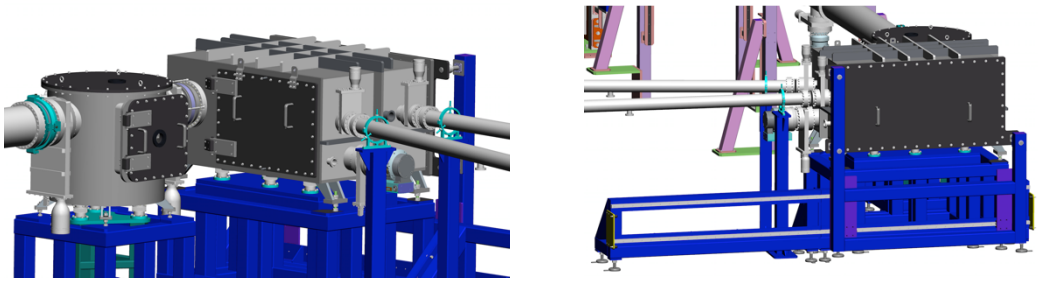

Figure 9: The Optical Chamber (rectangular tank) and the MM Chamber (cylindrical tank)

Inside the MM Chamber, the MMs are supported by an interfacing structure (Figure 10) designed to support the various MMs, which have different sizes, depending on their radial position inside the MAM. A reference area for the Effective Area measurements is also installed at this position.

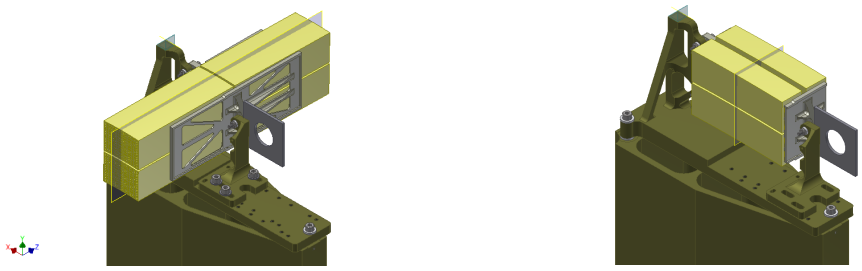

Figure 10: The MM interfacing structure

A thermal box, made in aluminum, surrounds the MM (Figure 11), and radiatively heats it, to test the optical properties at temperatures ranging from -10 to +50 °C. Liquid lines, connected to an external thermostat, modify the temperature of the thermal box. The liquid is flowing only in the edges of the thermal box, while the radiating panels are conductively heated/cooled. Two panels can be removed, to obtain some temperature gradients on the MM itself. A detailed description of the thermal box and its thermal simulations can be found in [21].

Figure 11: Thermal box. Left: schematic drawing. Right: the thermal box surrounding the MM, positioned on its interface piece, and on the motorizations.

4.4 Long arm

The long arm propagates the focusing beam from the MM to the detector (Figure 12 left). The arm is connected to the MM chamber by a cardanic off-loading mechanism (Figure 12 right), which enables the tube movements in vertical and horizontal directions. The downwards movement, to -1.4 m, is used for the detector to follow the focused beam, directed downwards by the double reflection on the MM, with an angle determined by the radius of the MM.
A lateral movement guarantees the uniformity and collimation measurement of the entire beam.
The tube is composed of 6 sections in order to make possibly future changes in the facility. The long arm is supported and moved by the detector tower; additional supports are used to unload the mass.

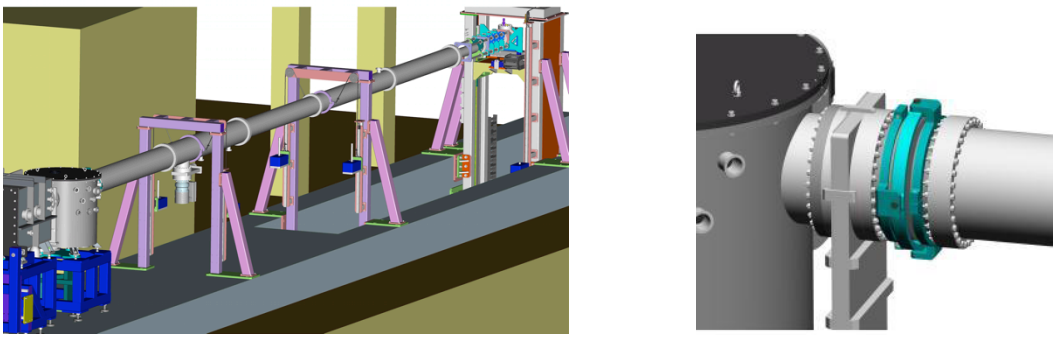

Figure 12: The long arm with it supports. Right: the cardanic mechanis

4.5 Detector tower

A more robust design, with respect to the one presented in previous papers [9,10] was chosen at the detector side. In the preliminary design, the detector was flanged to the long arm and the focusing was performed by moving the MM. In the present solution, the CCD is moved by in air motorization (translations X,Y,Z), installed on the detector tower (Figure 13), a solid structure, fixed to the foundation. The detector is connected to the long arm by four bellows, guided by a four bars structure, which allow the focusing of the image. A cold finger is placed in front of the camera, and kept at a temperature lower than the CCD, to avoid condensation on the CCD sensor.

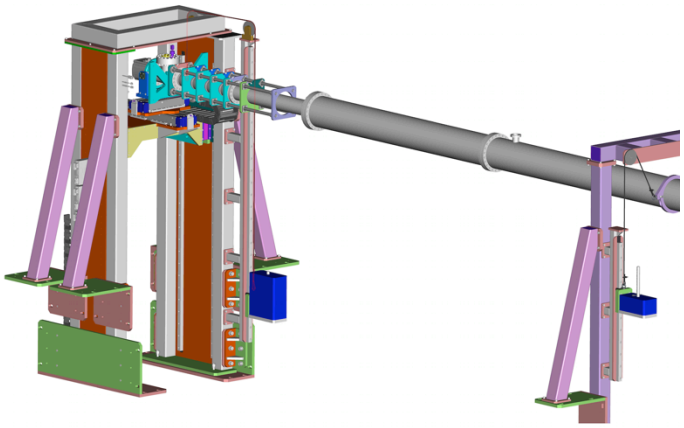

Figure 13: The detector tower, and the four bars guiding system of the bellows

5. VACUUM PUMPING SYSTEM

As already anticipated, the vacuum system is designed with modular compartments where the vacuum can be broken independently. This is primarily important for the MM replacement, in order to guarantee the test rate of 3 MM/day.

The design of the vacuum pumping system is carried out with the following goals:

- minimize vibrations
- compatibility with a vacuum level of 10^{-6} mbar; operations at 10^{-3} mbar
- evacuation time of the MM Chamber within 30 min
- evacuation time of the Optical Chamber, long arm, and short arms within 60 min (each sector separately)

To reduce vibrations, the following approach was considered:

- use magnetic turbo pumps (reduced vibrations with respect to mechanical turbo pumps)
- turbo pumps without fan (not necessary at the pressure considered; a water cooling system is already foreseen for these pumps)
- switch off the primary pump of the line during measurements

To implement these specifications, we have two vacuum lines:

1) pre-vacuum from 1000 mbar to 0.15 mbar with a single primary pump
2) high vacuum from 0.15 mbar to 10^{-4} mbar with magnetic turbo pumps

Two primary pumps are considered, one for the pre-vacuum line, the other one downstream the turbo pumps. Four turbo pumps are considered, two for the two short arms, one for the Optical Chamber, one for the long arm. Table 4 report the pumps selected in order to guarantee the requirements.

Table 4: Selected types of pumps

Item	Number	Type
Primary pump for the pre-vacuum line	1	Scroll 18 m^3/h
Primary pump for the turbo pumps	1	Scroll 40 m^3/h
TMP – Magnetic Turbomolecular Pump	3	Turbo mag int 300 l/s
TMP – Magnetic Turbomolecular Pump	1	Turbo mag int 600 l/s

The pumps and valves are operated under the control of gauges.
Venting is performed with N_2 for the Optical and MM Chambers, while filtered air for the arms.

6. ASSEMBLY INTEGRATION VERIFICATION

After the installation of the vacuum system the optical components will be pre-aligned with a visible light beam, while a fine alignment will be performed in X-ray. The parabola will be aligned to the X-ray source, using for the visible light a large laser beam in air. Then the alignment will be refined with X-rays in vacuum, by means of a Hartmann sensor flanged at the end of the Optical Chamber. The crystals of the monochromator will be aligned by maximizing the flux measured by an X-ray detector. A Hartmann plate, placed at the MM position, will allow us to perform the alignment of the beam expander, and the optimization of the alignments of all the optical components. Finally, it will be used to measure the collimation of the beam. The flux stability will be controlled by a beam monitor, palced in the Optical Chamber.

7. CONTROL SOFTWARE

The software, written in LabVIEW, controls the following components:

1) Vacuum system components (vacuum pumps, gates, valves, gauges), through controllers procured from National Instruments (NI)
2) Vacuum motorizations for the alignment of the optical components
3) X-ray source
4) CCD: acquisitions and motorizations
5) Beam monitor for X-ray flux stability control

The software will also monitor the status of the facility by data logging.
To anticipate the software development, prior installation of the vacuum system, a simulator was built (Figure 14) using a Raspberry Pi 3b+ minicomputer and two I/O boards (Figure 14 left), connected to the NI controllers and a monitor to visualize the state of the vacuum components (Figure 14 right), through virtual LEDs (for pumps and valves) and virtual switches (for the gauges and the feedback of pumps and gates).

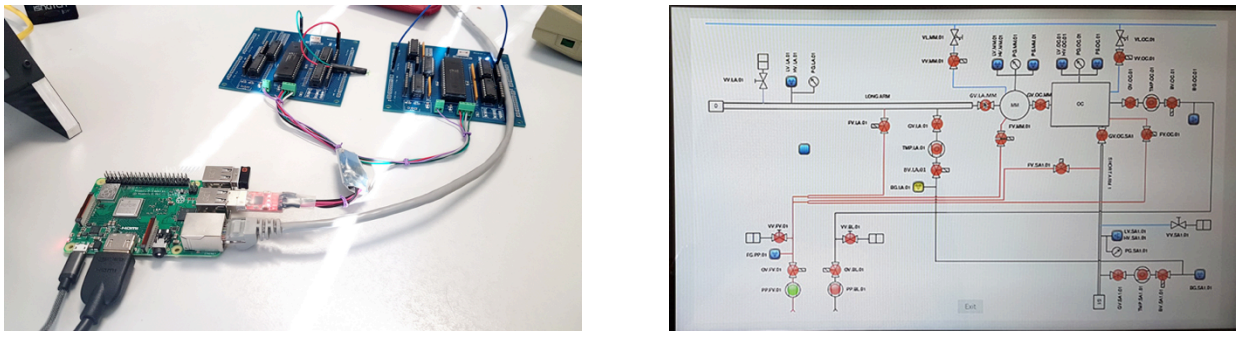

Figure 14: Vacuum system simulator. Left: the minicomputer connected to the I/O boards. Right: a virtual layout show the status of the vacuum components

8. CONCLUSIONS

The first beam line, at 4.51 keV, of the BEaTriX facility is under development at INAF-OAB, in its Merate premises. Thorough simulations have driven the error budget definition and the choice of the vacuum motorizations. The opto-mechanical design of the vacuum system was consolidated, introducing some modifications in order to make the system more robust: the major changes in the design have been introduced to allow the movement of the detector and the X-ray source. The procurement of the vacuum motors and the vacuum system is on going. The X-ray source is being developed by Incoatec and will be completed by Gilardoni: the preliminary results obtained by Incoatec are very positive and satisfy the requirements. The parabolic mirror polishing at INAF-OAB is giving very positive results. The crystal in Silicon for the beam expander was recently measured at IMEM-CNR who reported a planarity as perfect as one can measure with the standard techniques. They have also tested the ADP crystal needed for the 1.49 keV beam line, reporting very good crystal quality. The procurement phase of all the needed components is on going. A control software in LabVIEW is under development with the help of a vacuum simulator developed ad hoc to test it before the installation of the vacuum system. The system is expected to be ready in Q4 2020.

ACKNOWLEDGMENTS

The development of the BEaTriX facility is funded by the ESA contract No. 4000123152/18/NL/BW, “Advanced and Compact X-ray Test facility for the ATHENA SPO module”, the AHEAD consortium activities financed by the EU Horizon 2020 grant No. 654215, and INAF internal funds. We thank Paolo Conconi for his guidance and assistance in the project. Marco Riva and Matteo Aliverti are also acknowledged for help and support.

REFERENCES

[1] Nandra, K., Barret, D., Barcons, X., et al., "The Hot and Energetic Universe: A White Paper presenting the science theme motivating the Athena mission", http://arxiv.org/abs/1306.2307 (2013)
[2] Bavdaz, M., Wille, E., Ayre, M., Ferreira, I., Shortt, B., et al., "Development of the ATHENA mirror," Proc. SPIE, 10699, 106990X (2018)
[3] Collon, M., Vacanti, G., Barriere, N., Landgraf, B., Guenther, R., et al., "Silicon pore optics mirror module production and testing," Proc. SPIE, 10699, 106990Y (2018)
[4] Krumrey, M., Muller, P. et al., "New X-ray parallel beam facility XPBF 2.0 for the characterization of the silicon pore optics," Proc. SPIE 9905, 99055N (2016)
[5] Vacanti, G., Collon, M.J., Barrière, N.M., Landgraf, B., Günther, R., et al., "X-ray testing of Silicon Pore Optics," Proc. SPIE, this conference, (2019)
[6] Valsecchi, G., Bianucci, G., Marioni, F., Zocchi, F.E., et al., “Integration facility for the ATHENA telescope,” Proc. SPIE, this conference, (2019)
[7] Burwitz, V., Bradshaw, M.J., Eder, J., “PANTER activities toward testing and calibrating ATHENA optics,” Proc. SPIE, this conference, (2019)
[8] Moretti, A., Pareschi, G., Uslenghi, M., Sironi G., Tordi, M., et al., “VERT-X: a VERTical X-ray rasterscan facility for calibrations,” Proc. SPIE, this conference, (2019)
[9] Salmaso, B., Spiga, D., Basso. S., Ghigo, M., Giro, E., Pareschi, G., Tagliaferri, G., Vecchi, G., et al., “Progress in the realization of the beam expander testing x-ray facility (BEaTriX) for testing ATHENA’s SPO modules,” Proc. SPIE 10699, 1069931 (2018)
[10] Salmaso, B., Spiga, D., Basso. S., Ghigo, M., Giro, E., Pareschi, G., Tagliaferri, G., Vecchi, et al., “BEaTriX (Beam Expander Testing X-ray facility) for testing ATHENA’s SPO modules: advancement status,” Proc. SPIE International Conference on Space Optics 2018, Vol. 11180, 1118026 (2019)
[11] Spiga, D., Pareschi, G., Pelliciari, C., et al., “Functional tests of modular elements of segmented optics for x-ray telescopes via an expanded beam facility,” Proc. SPIE 8443, 84435F (2012)
[12] Spiga, D., Pelliciari, C., Bonnini, E., et al., "An expanded x-ray beam facility (BEaTriX) to test the modular elements of the ATHENA optics," Proc. SPIE 9144, 91445I (2014)
[13] Pelliciari, C., Spiga, D., Bonnini, E., et al., “BEaTriX, expanded soft x-ray beam facility for test of focusing optics, an update,” Proc. SPIE 9603, 96031P (2015)
[14] Spiga, D., Pelliciari, C., Salmaso, B., et al. “Design and advancement status of the Beam Expander Testing Xray facility (BEaTriX),” Proc. SPIE 9963, 996304 (2016)

[15] Burwitz, V., Willingale, R., Pareschi, G., et al., "AHEAD joint research activity on X-ray optics," Proc. SPIE 10699, 106993T (2018)
[16] Sanchez del Rio, M., Cerrina, F., "Asymmetrically cut crystals for synchrotron radiation monochromators," Review of Scientific Instruments 63, 936 (1992)
[17] Ferrari, C., Beretta, S., Salmaso, B. , Pareschi, G., Tagliaferri, G., et al., "Characterization of ADP crystals for soft x-ray optics of the Beam Expander Testing X-ray facility (BEaTriX)," Journal of Applied Crystallography, 52, 599-604 (2019)
[18] Spiga, D., Salmaso, B., Basso, S., Bavdaz, M., Burwitz, V., et al, "Optical simulations for the laboratory-based expanded and collimated x-ray beam facility BEaTriX," Proc. SPIE, this conference, (2019)
[19] ATHENA CDF study report. Assesment of an X-ray telescope for the ESA Cosmic Vision Program, (2014)
[20] Vecchi, G., Salmaso, B., Basso, S., Sironi, G., Ghigo, M., Spiga, D. et al., "BEaTriX, the Beam Expander Testing X-ray facility for testing ATHENA's SPO modules: the collimating mirror," Proc. SPIE, this conference, (2019)
[21] Basso, S., Salmaso, B., "Thermal simulations of the ATHENA Mirror Modules to be optically tested in the BEaTriX facility," Proc. SPIE, this conference, (2019)